CHALMERS
UNIVERSITY OF TECHNOLOGY

Bio-Inspired Transportation Network Optimisation

Reinforcement Rules in Physarum Vein Networks

Complex Adaptive Systems

Louis Etienne Devers

Bio-Inspired Transportation Network Optimisation

Reinforcement Rules in Physarum Vein Net

LOUIS Etienne DEVERS

Bio-Inspired Transportation Network Optimisation
Reinforcement Rules in Physarum Vein Networks
Louis Etienne Devers

Cover: Flow within Physarum Polycephalum's veins visualised by fluorescent beads using a confocal microscope. Images extracted from our experiment.

Bio-inspired Transportation Network Optimisation
Reinforcement Rules in Physarum Vein Networks
LOUIS DEVERS
Department of Physics
Chalmers University of Technology

Abstract

The decision making process of unicellular organisms such as the amoeba *Physarum polycephalum* may represent primitive forms of computation. Such non neuronal organisms exhibit complex optimisation behaviour, apparently solving NP hard problems in linear time. Understanding such behaviour may be relevant for many different fields besides biology, from metaheuristics to neuroscience or information theory. This master thesis explores possible reinforcement mechanisms *Physarum polycephalum* that influence vein network formation and biomass density distribution. The state-of-the-art *Flow Conductivity Model* (Tero et al 2006) that describes vein development will be tested for the first time experimentally using time-lapse-imaging-techniques. If this model (also called the *Physarum Solver*) is the one used to reproduce the slime mold's solving capacities it lacks many of the Physarum's biological features, such as growth. However, we show that the Physarum expansion neglected by the Flow Conductivity Model was not necessary, as the order in which food sources were met did not influence the final distribution of biomass. By using fluorescence microscopy, we have been able to quantify the flow within the veins of the slime mold, extracting both the local diameter and the local flow rate within the veins. We notes that the contractile cycles missing from the model may have a strong impact on the decision making process. The fast contractile cycle creates the flow by dilating the vein and creating low-pressure points; while the phase of the slow contractile cycle distinguishes veins that will be reinforced from the other veins. The fit to the empirical data has a different form to the various model functions that have been used. However, even if the model does not fit experimental data trend, it still has utility for bio-inspired optimisation and pedagogical purposes. Furthermore, the Flow Conductivity Model may give us a better insight of the mechanic of the slime mold's vein selection than a new model over-fitting experimental data.

Keywords: slime mold, physarum, emergence, venation, Flow Conductivity Model, optimisation, transportation, bio-inspired networks.

Acknowledgements

Contents

List of Figures

List of Figures

1

Introduction

Transportation networks balancing efficiency, cost and resilience are complex to optimise and yet, this optimisation is commonly observed in nature [2]. For example, the efficient venation of a plant is a fundamental element for its survival[3]. Such biological networks emerge from evolutionary pressure, depending on their environment and needs. The architecture of the biological network is then linked to its function and its fitness.

In nature, dynamical graphs can also be observed, as in neuronal networks, fungi, ant colonies, and protists. These networks need to be rearranged continuously, are resilient to damage, and cost-efficient[4]. More importantly, the architecture of the network depends on a local decision making process, and not solely on evolutionary pressure [5]. The architecture of the network can then be seen as a coherent whole emerging from local decisions [6].

Mathematical modelling and simulation of such dynamical networks is of interest to aid understanding of biological systems. Furthermore, the local decision making rules could also be relevant in bio-inspired metaheuristics like the Ant-Colony Optimisation Algorithm [7]. Indeed, combining these rules can lead to the emergence of behaviours that solve complex problems in a linear time scale [8].

This thesis is primarily aimed at applied physicists and mathematicians, but also biologists having an interest in modelling dynamical networks.

1.1 Context

The protist *Physarum polycephalum* builds dynamical networks of veins between food sources to transport its nutrients [9]. The networks built by the Physarum can solve complex optimisation problems such as the Steiner Tree Problem [10], the Shortest Path Problem [11], or the Travelling Salesman Problem [8].

The dynamical selection of veins in the Physarum network has been modelled assuming hydraulic coupling and a Poisseuille flow[11]. In this model, the veins are positively reinforced by the flow passing through them, while being subject to a constant decay term. This model effectively mimics Physarum capacity to solve certain problems by giving similar outcomes in vein patterns to optimal solutions [12].

1.2 Problem statement

While the models efficiently reproduce and applying the dynamical selection properties of the Physarum between food sources [13], little is known about the actual

reinforcement mechanism of the veins [14]. Whilst the outcomes of the model are relatively similar to the actual network [5], the reinforcement rules proposed have never been directly related to experimental data. Our **global working question** is thus: What is the reinforcement process in Physarum's decision making? Two sub questions arise :

- **Sub Question 1**: Is the reinforcement sensitive to initial conditions or timing of resource encounter?
- **Sub Question 2**: Is the current reinforcement model consistent with the experimental data? If so, what are the parameters providing the best fit?

1.3 Purpose

The purpose of this thesis is to propose experimental protocols and mathematical tools that underpin Physarum's vein selection. This work has been carried to quantitatively compare the model with experimental data, and propose bio-mimetic rather than bio-inspired alternatives.

1.4 Limitations

This thesis does not contain graph theoretic measurements of the resultant network. Networks have been extracted using image analysis, but in the sole purpose of analysing each vein as an individual influenced by its radius and flow. Although the network is sensitive to many factors covered in the literature: no variation in resources, heat, or light exposure were tested.

2

Background

This chapter outlines the biology of the Physarum, the mathematical model involved, and the time-lapse-imaging protocol.

2.1 Physarum polycephalum

In this section the Physarum polycephalum (slime mold) and its problem solving capacity are introduced.

2.1.1 Physarum as a single celled amoeba

2.1.1.1 Growth forms and habitat

The *Physarum polycephalum* is an amoeboid organism living in damp and dark areas such as forests. It can be found in America, Europe, Japan and Australia as a yellow mass crawling on dead logs or leaves. It is unicellular but possesses many nuclei and is most frequently observed in the form of a plasmodium (Fig2.1). Its plasmodium spreads like a liquid in a fluvial manner to explore its environment, foraging for food at up to $4\,\mathrm{cm/h}$ [9]. It mainly eats dead bacteria, but also appreciates mushrooms and oat flakes. It produces enzymes to digest the food and sub-

Figure 2.1: Physarum polycephalum foraging food

sequently absorbs the nutrients. The slime mold usually forms networks of veins between the food sources to transport the resources throughout the organism.

2.1.1.2 Vein formation

The slime mold's size can be important, and thus diffusion alone cannot support nutrient distribution across the whole organism. The plasmodium tends to contract and form veins, pumping resources through its whole body. The flow is carried by contractile cycle of the veins with a period of about $120\,\mathrm{s}$. The flow within these veins goes back and forth, reversing its orientation within each cycle. This flow is characterised as *Shuttle streaming* [11, 15].

2.1.2 Computing capacity

Similarly to plants, the vein network must be efficiently routed to find a trade-off between transport capacity, and resilience to damage [16, 5]. This dynamical wiring between food sources is of high interest, as its modelling could help solve other de-centralized transportation optimisation problems. As the slime mold is a non neuronal organism, it musts only rely on locally sensed information to build its network. This emergent phenomenon of vein selection has been used to propose solutions to routing problems. In particular, the slime mold provided good answers for the Tokyo railway network [5], the shortest path problem [17], mazes [11], nutritional trade-offs [9], or the travelling salesman problem [8].

2.2 Flow Conductivity Model

In this section, the Flow Conductivity Model introduced by Tero et al [5] [11] will be presented.

2.2.1 A physical system

2.2.1.1 A planar mesh of vein

The plasmodium is abstracted as a planar Delaunay mesh of veins between nodes. Each vein has a conductivity D_{ij} randomly and uniformly distributed between 0.5 and 1 initially. The conductivity can be described as the capacity of a pipe to carry a flow (). The model assumes Poisseuille flow, which computes the conductivity D_{ij} as follows :

$$D_{ij} = \frac{\pi R_{ij}^4}{8\xi} \tag{2.1}$$

Here R is the radius of a pipe (here a vein) and ξ is the viscosity of the fluid going through this pipe.

2.2.1.2 Food sources displayed on the mesh

Food sources are abstracted as node locations which can apply pressure to the system, thus creating a flow. In this model the flow distribution is approximated by selecting two food sources at each time step. The first one is selected completely randomly, and the second one is also selected randomly yet preferentially far from the first one [12]. The first and second nodes selected will apply in and out flows I_0 and $-I_0$ respectively, a source and a sink. Then, the flow rate Q_{ij} between all the connected nodes i and j can be calculated as :

$$Q_{ij} = \frac{D_{ij}}{L_{ij}} (p_i - p_j) \tag{2.2}$$

Where Q_{ij} is the flow rate, L_{ij} is the length of the vein and p_i is the pressure at node i.

2.2.1.3 Solving the flow and pressure

However, both the pressure and the flows are unknown and need to be computed, which is done by solving the system using Kirchoff's law. Namely, the sum of in and out flows is null for all nodes, except for the sink and the source nodes which have flows of I_0 and $-I_0$, respectively :

$$\sum_i Q_{ij} = \sum_i \frac{D_{ij}}{L_{ij}}(p_i - p_j) = \begin{cases} I_0, & \text{for } j = 1 \\ -I_0, & \text{for } j = 2 \\ 0, & \text{otherwise} \end{cases} \tag{2.3}$$

This operation is usually carried using inversion or pseudo-inversion of a matrix to compute p and then deducing the flux Q_{ij}. This computation is typically time consuming, and represents most of the computational cost of this algorithm.

2.2.2 The current reinforcement system

2.2.2.1 General function

Each flux can be computed between all nodes i and j, but the final output of this algorithm is based on the conductivity which varies over time. The conductivity evolves positively (reinforcement) or negatively (decay) for each vein at each time step. A reinforced vein will become bigger and have a higher flux, meaning that its conductivity is higher than the other veins. Tero et al proposed a reinforcement of this conductivity based on the flux as follows :

$$\frac{dD_{ij}}{dt} = f(|Q_{ij}|) - \alpha D_{ij} \tag{2.4}$$

Where the conductivity is updated by a function of the absolute flow through its vein, thus independently of its direction. The conductivity is subject to a decay term, α, effectively decreasing the radius of veins with low flow. This reinforcement rule is close to the Ant Colony Optimisation reinforcement rules, except the latter model a decaying pheromone trace instead of a decaying conductivity [7].

2.2.2.2 Different functions

Many reinforcement functions have been proposed, such as :

$$f(|Q_{ij}|) = \begin{cases} |Q_{ij}| \\ |Q_{ij}|^\mu \\ \frac{Q_{ij}^\mu}{1+Q_{ij}^\mu} \\ \beta|Q_{ij}| \end{cases}$$

However, none of these functions have been experimentally established, and are used for their convenience when applied to different routing problems[11]. This lack of biological evidences in the reinforcement rules motivates the new time-lapse-imaging

protocol based on tracking fluorescent beads that we developed during this thesis. The aim of this experiment is to quantify the flow within a vein using fluorescent beads simultaneously with the local vein diameter.

2.3 Fluorescence and tracking

In this section, previous uses of fluorescence in Physarum are described briefly. However, most of the flow measurements and forces quantification have been carried on other slime molds such as the Dictyostelium, or on way smaller scales. This is why the protocols used on Dictyostelium, another kind of slime mold, can be of interest. Most studies only contain one fluorescent bead tracked, where ours is simultaneously tracking an important quantity in real time.

2.3.0.1 Uses of fluorescence in Physarum

Fluorescence has already been used in Physarum, but mainly to label anatomical elements [18], or to facilitate image processing [19] by labelling the cellulose for instance [20]. There are very few experiments using fluorescent beads to track the flow in the Physarum, and neither uses the scale we used during this thesis. For example, ground forces applied by the Physarum have been quantified using fluorescence and traction force microscopy [21], but in a slime mold measuring only $100 \, \mu m$, where in ours measures approximately $5 \, cm^2$. This protocol could not be applicable at our scale, since we must gather data from several veins, while a single vein is about $100 \, \mu m$.

2.3.0.2 Single bead tracking

Alim et al [14] tracked the movement of a fluorescent bead (of $1 \, \mu m$) through a single isolated vein of Physarum over a short period of time, to link contractions and flow within a single vein. This experiment is very similar to ones done on Dictyostelium with several beads tracked through a Dictyostelium slug [22]. However, the mechanism transporting the bead is different, as Dictyostelium is a cellular slime mold.
Other experiments used single beads methodology to underline wave behaviour in Dictyostelium, which could be of interest since Physarum possess similar cyclic features [23, 24]. However, single cell tracking would not be sufficient since many different paths could be used in a late-state Physarum network to go from a certain location to an other. To quantify both the flow and the conductivity, this thesis required a novel flow quantification protocol, using multiple beads and parallel morphological measurements.

3

Method

In this chapter we present the two protocols used during this thesis. The first protocol consist of a time lapse of 60 hours of a slime mold covering a 2.5 cm diameter disk of 2% water-agar medium to examine timing and initial conditions of the reinforcement. The second protocol is a time lapse of half an hour acquired using a confocal microscope to relate the flow the flow reinforcement model to empirical observations. Both protocols include image analysis and quantification of the results.

3.1 Density and occupation ratio

This section will focus on the first experimental protocol concerning the growth of a single slime mold on a petri dish. Food Sources (FS) were distributed evenly around the periphery of the dish, and the decisions of the slime mold were quantified by the area it occupied [9]. The local biomass distribution was estimated by the intensity of the light at each point. Thus, a dark area has more slime mold than a light one, according to the Lambert-Beer Law (assumed here).

3.1.1 Hypothesis and research question

The reinforcement of the slime mold allows it to form veins between food sources [5]. The occupation of a food source is a choice made by the slime mold, as the area occupied is relative to its resource needs [9]. Local reinforcement rules, redirecting the flow for instance, could potentially bias the decision by preferring first-met food sources. This bias can be interpreted as a sensitivity to initial conditions as shown in Fig 3.1. The working hypothesis is that the occupation is uniform over the dish after an extended time. Rejecting it would underline a sensitivity to initial conditions in the resulting network.
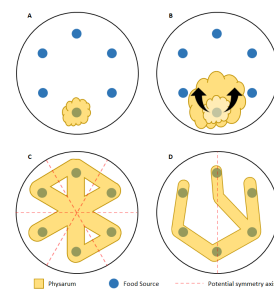
Figure 3.1: Asymmetric occupation of the medium

3.1.2 Material and procedure

This subsection gives a brief description of the methodology for the slime molds experiments.
The typical growth of a slime mold in this experiment can be seen in Fig3.2. 60 independent experiments were executed. In each experiment, a volume of slime mold

Example of exploration over time
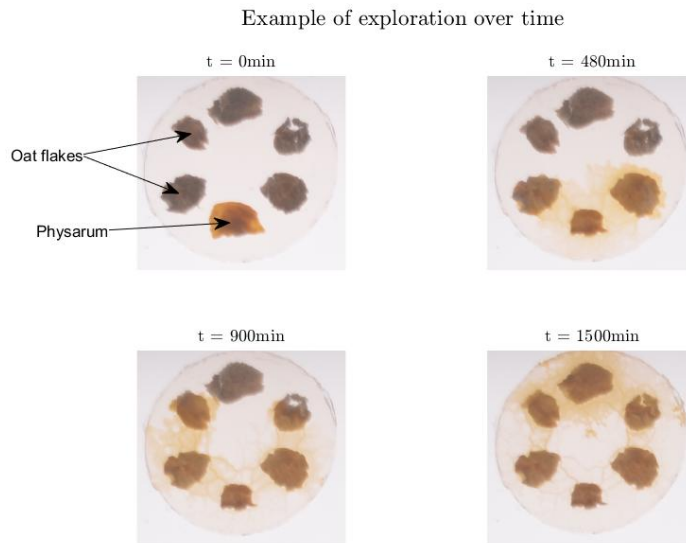
Figure 3.2: Example of typical slime mold growth in this protocol

(25.2 ±7 mg) was positioned in a 2.5 cm diameter disk of 2% water-agar medium with 6 food sources (Quaker® oat flakes). Before the experiment, the slime mold has been sub-cultured in a similar concentration medium and fed twice a day with Quakers oat flakes. The subcultures were maintained in 20 by 20 cm petri dishes until the slime molds were ready for experiment, usually after one or two weeks.

Once they produced a thick and even frontal growth wave, thin cuts perpendicular to the growth front were made using a scalpel. Each cuts were roughly 7 mm apart and approximately 20 mm long. Each rectangular section of the slime mold was then transferred to a new medium using a semi-rigid plastic sheet of the same size to make a spatula. The spatula must slide between the slime mold and the medium without collecting any medium, bias the weight measurements, or damaging the slime mold. Any slime mold damaged by this process were excluded form the experiment.

The slime mold was placed on one of the 6 food sources which were positioned in a concentric manner, forming an inner disk of diameter 1.5-1.75cm. Each run was then conducted in an opaque black box illuminated by an electro-luminescent sheet at room temperature (21°C). A Canon camera was set to take picture every 3 minutes for 60 hours.

3.1.3 Data and Image Analysis

The aim of this subsection is to introduce the image analysis techniques that were used to segment the physarum and the oat flakes. It will also cover the quantification used to compute the *Occupation ratio* presented in the results chapter.

3.1.3.1 Enhancing the contrast

Once the time lapse data were acquired, images were analysed using Matlab. Each object present namely background, the food sources, and the slime mold, have a

specific colour. This colour difference was enhanced and used to differentiate each component reproducibly.

t = 831min
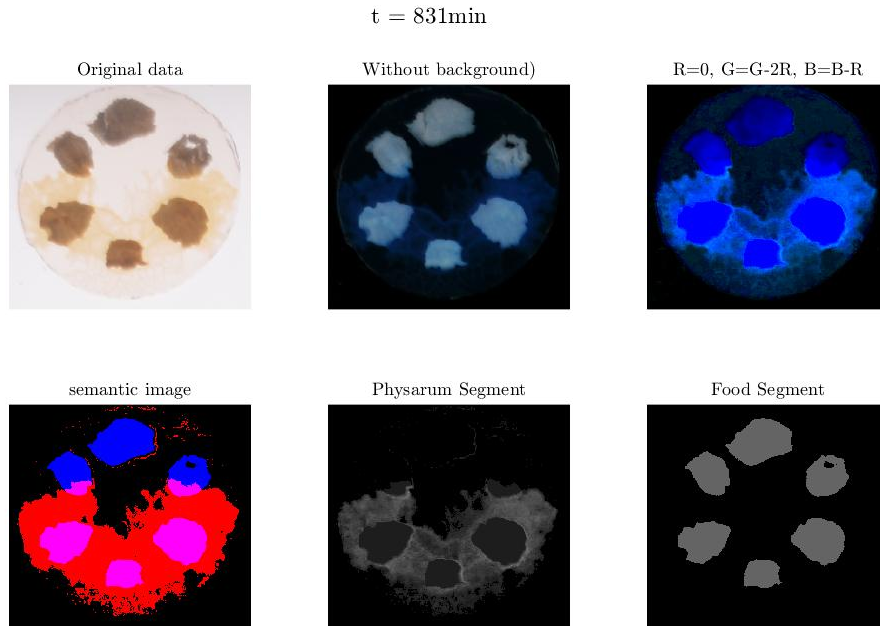
Figure 3.3: Segmentation steps to differentiate semantic elements

The background was subtracted by taking pictures of the EL sheet before introduction of the dishes. Each colour channel from the background-free image (bf), namely Red, Green and Blue (R_{bf}, G_{bf}, B_{bf}), were modified to enhance the Physarum image, as follows:

- $R_e = 0$
- $G_e = G_{bf} - 2R_{bf}$
- $B_e = B_{bf} - R_{bf}$

Here R_e, G_e, and B_e are the red, green and blue enhanced channels respectively in figure 3.3. Note that these operations on the colour channels were found empirically.

3.1.3.2   Segmentation

The enhanced images were then segmented to efficiently select the Physarum position and density over time. The enhanced image was averaged to a single grey level image and segmented using Otsu Thresholding [25]. The Otsu binarization is assuming a bi-modal distribution of pixel intensity in the image histogram. This is the case here, as a background component and a foreground component can be easily distinguished in Fig3.3. The Otsu binarization algorithm finds a threshold value splitting the image histogram into two components. The pixels above or under this threshold will become 1 or 0 respectively. This optimal threshold minimises the intra-variance of the two components, fitting a bi-modal distribution of pixel intensity. A similar segmentation was also done to the food sources without any prior enhancement.

3.1.3.3 Occupation ratio

The position of the slime mold was quantified from the segmentated image. Assuming a Lambert-Beer law relationship between biomass and light transmission. The higher the light intensity is in the inverted Physarum segment picture (Fig3.3), the denser the slime mold is at this location. This allowed a quantification of the slime mold's biomass distribution over the dish. We assumed that the distribution of light intensity was a reasonable quantification of the slime mold's mass or decision, as it has been successfully used previously [9, 26] In order to generalise the data from an experiment to another, each dish was virtually clustered in 6 classes corresponding to the area surrounding the 6 oat-flakes. The distribution of the mass is then clustered to 6 these classes as a ratio r_i such as $\sum_{i=1}^{6} r_i = 1$. The ratio was normalised by the size of the classes, as some areas surrounding flakes are bigger than others. Considering that Lambert-Beer law does not apply through opaque objects, the oat-flake itself was discarded from each area.

3.2 Flow quantification

This section describes the protocol used to compare the Flow Conductivity Model with empirical data [5, 11, 26, 10]. This section gives further understanding of the results, while giving insights of the methodology used. In order to compare the Flow Conductivity Model to the actual flow reinforcement rules in the Physarum, we used time-lapse microscopy of $1\,\mu m$ fluorescent beads taken up by physarum, and image analysis to extract the vein diameters and flow rate.

3.2.1 Hypothesis and research question

The Flow Conductivity Model consists of a reinforcement of the conductivity of the veins in response of the internal flow rate. To compare the model to the empirical data, an estimation of the actual conductivity and flow rate in continuous time is necessary.

3.2.2 Material and procedure

3.2.2.1 Time-lapse imaging

A subset of veins are visualised using microscopy. A $20\,mg$ slime mold was placed on a 2% water-agar medium $24\,h$ before the experiment without any food sources. It has been exposed to a solution of $1\,\mu m$ fluorescent beads diluted in water at the same time. After this time, it spread to an area of approximately $5\,cm^2$ forming thin veins networks. Using a $\times 32$ magnification, both the veins and their flow are visible.

3.2.2.2 Measurements of the flow

The flow is relative to the velocity vector, and to obtain such a vector we used imaged $1\,\mu m$ fluorescent beads in fluorescence and vein morphology in bright field

over a 30 minutes time period. After each bright-field image, two fluorescent images at different exposure times were taken. The first was short (0.2 s) and created a sharp point. Superposing these points with the veins showed the position of all the beads in the veins, here visualised in red in Fig 3.4. The second lasted 5 s, and was done with a dimer excitation light to compensate for the longer time of exposure. It produced a streak giving us the absolute speed (norm of the velocity vector) of any given beads, represented in green in Fig 3.4. Having the absolute value, and also the direction of the beads, we can reproduce the flow vector field within the veins.
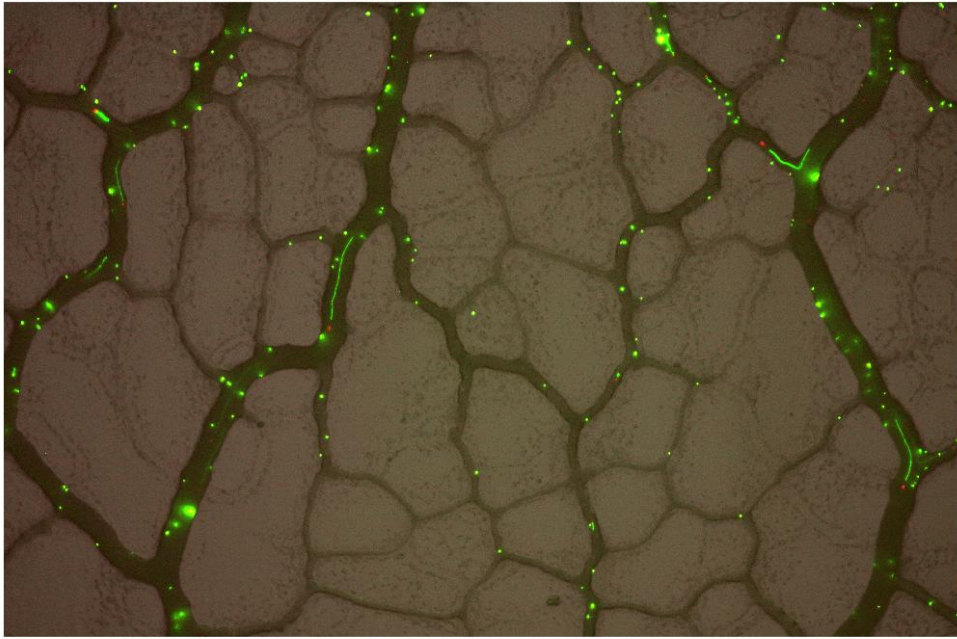
Figure 3.4: Bright-field and fluorescent channels superposed giving flow vectors

3.2.3   Data and Image Analysis

The original time lapse video data was approximately 20 GB for a 30 min experiment. The images at each time point were segmented using Matlab to obtain :

- an abstraction of the vein network, namely position and connectivity of the different edges/veins.
- a matrix $R_{ij}(t)$, the radius of the vein section ij between nodes i and j for all time steps t.
- a matrix $v_{ij}^{max}(t)$, the fastest bead observed in the vein section ij between nodes i and j for all time steps t.

3.2.3.1   Segmentation of the vein network

The radius of each vein $R_{ij}(t)$ is the key elements required to compute their conductivity $D_{ij}(t)$. To obtain R_{ij}, we used different image analysis techniques to create

a binary mask of the veins. The measurements were then done directly using this mask superposed dynamically on the veins for all time steps. However, to aggregate the mixed data for each vein, it is important to have the connectivity matrix of the vein network, to discriminate each vein separately.

The veins can be considered as multi-scale ridges that can be efficiently segmented using a Frangi Vesselness filter [27]. The computational cost of such filter is relatively high, but the results were better than with adaptive thresholding or edge detection filters. However, the inside of thick veins was not recognised correctly as a vein by the Frangi filter, so operations such as morphological closing (dilation followed by erosion) and selection by connected elements were added to obtain a correct mask. This method has been applied successfully to all the time steps, giving a binary mask for the veins.

The skeleton of the network was extracted by generating a composite minimum intensity projection of the vein over time, giving the largest network of veins that could be observed. Effectively, the presence of a vein was noted by a darker bright-field pixel during the parts of the time course, independently of whether they subsequently disappear.

By morphological thinning and spurring, the mask composed a consistent network of veins that can disappear over time and still be formally considered. Nodes have been added at extremities or intersections, giving an abstraction of the network as in Fig3.5. However, this thesis is not focused on individual nodes, but on the veins sections between them.
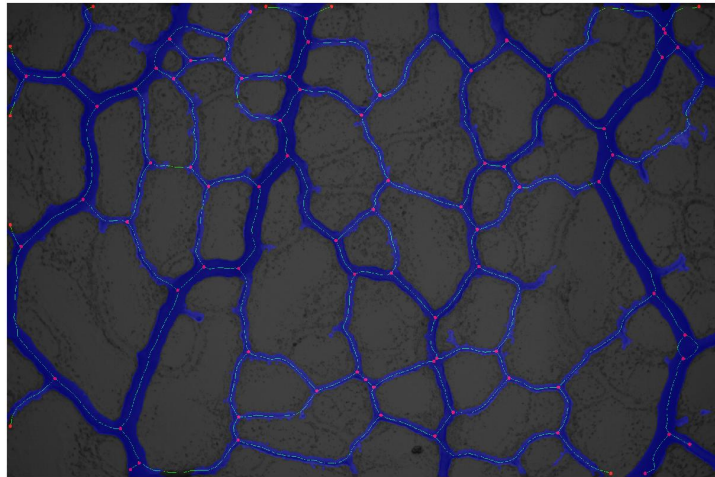
Figure 3.5: Network extracted

3.2.3.2 Radius measurement and correction

The radius is estimated using the segmentation mask as seen in blue in Fig3.5. Each pixel is related to its closer vein, giving thus an area A_{ij}. The length L_{ij} of each vein is evaluated by measuring the length of the skeleton in green Fig3.5 between

nodes i and j. The radius R_{ij} is firstly estimated as : $R_{ij}(t) = A_{ij}(t)/L_{ij}$ but can be noisy and will be improved.

As the segmentation can erode some veins under a certain size completely, the radius estimated from the binary mask falls as in Fig 3.7. As the derivative of the conductivity is the output of the Flow Conductivity Model, it is necessary to have a smooth and precise radius for these points.

In Fig 3.6, we can note that the erosion of certain veins leads to diameters of 0. To estimate the correct radius from these noisy measurements, we compared the bright-field intensity values of each veins with their segmentation radius (Fig 3.6). The thickness of a vein was estimated by how dark it appears on the picture, assuming a Lambert-Beer law. From this, we used a robust linear regression for each vein, to estimate the segmentation radius based on their bright-field values. The illumination was not uniform accross the field. So each vein required its own linear regression parameters to increase accuracy (each colour represents a separate vein in Fig 3.6). The robust linear regression trained on the noisy segmentation radius provided smooth and reliable estimation of the actual radius, now relying on the bright-field intensity rather than the segmentation process. The estimation was temporally arranged using a moving-mean smoothing filter. This filter prevented dD_{ij}/dt to be too sensitive, to give the final radius $R_{ij}(t)$.
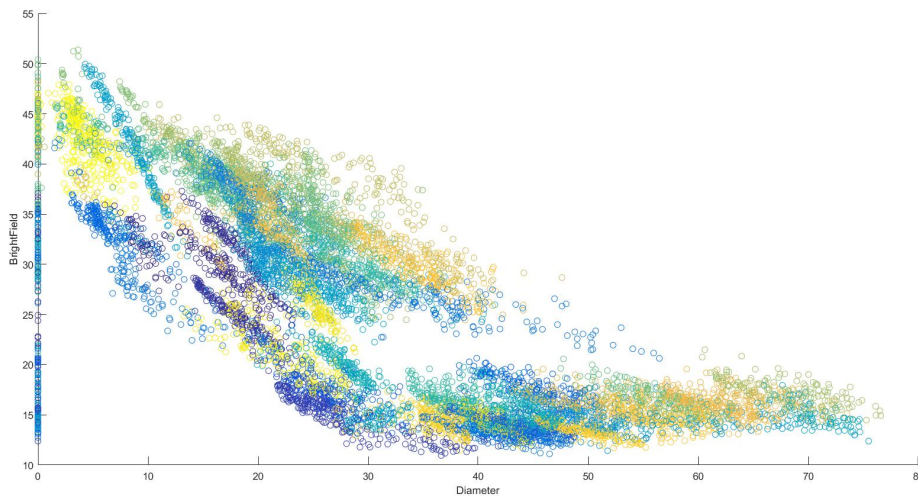
Figure 3.6: Individual vein's linear relationship between diameter and bright-field

3.2.3.3 Segmentation of the beads

The short and long exposure fluorescent images (respectively red dot and green streak in Fig3.4), needed to be segmented to extract the speed, direction and location of all the beads. Some beads remained stuck in the plasmodium without being carried by the flux. These were ignored using the time differential : $im_{diff}(t) = \max{(im(t) - im(t-1), 0)}$. Where $im(t)$ is the image at time t. The segmentations were done using this differentiated time series, allowing to effectively clean both channels from non-moving components.
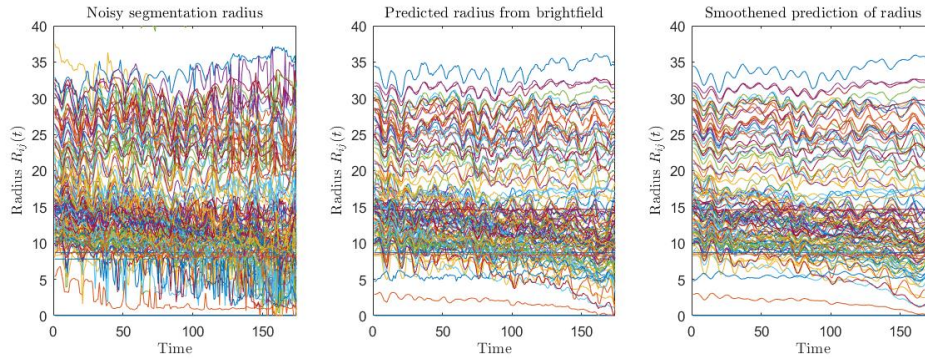
Figure 3.7: Radius correction steps

Both channels must be segmented to avoid type 1 and type 2 errors in our masks, but the input signal was noisy. The short exposure channel (red dot in Fig 3.4) was cleaned using Wiener filtering [28] and segmented using adaptive thresholding. The long time exposure (green streaks in Fig 3.4) was similarly cleaned using a Wiener filter, and the streaks were detected using a Sobel-Feldman operator [29]. The correction of the resultant binary mask used morphological closing, and deletion of small connected components.

At this point, the links between the dots and the streaks were not made, and throughout this thesis, only the lengths of the streaks will be used to estimate the absolute flow $|Q_{ij}|$ and not the actual oriented flow Q_{ij}. Nevertheless, using the x and y coordinates of the segmented streak can give an estimation of the possible location needed to determine orientation. We carried out polynomial regressions of degree 2, assuming that a bead could not change its direction more than once in a single time step, to estimate the red dot location. By knowing the exposure time, and the delay between the two channels, reasonable estimations of orientations were made. However, coupling each dot to each streak is a computationally slow task, and was not implemented during this thesis, as the model only needs the absolute flow and not its orientation.

3.2.4   Relation to the mathematical model

We assumed that the flow was turbulence-free, that maximum flow was observed in the middle of the veins, and the veins frame circular cross-section. To compute the flow within the veins, we are assume a flow following Hagen-Poisseuille flow. The flow should indeed be laminar as the density and viscosity of the fluid flowing within the veins is of the same order as water. Further details are in the Result section.

4

Results

4.1 Timing and resource related reinforcement

This section describes the results obtained from the first experimental protocol, involving a slime mold in an arena with 6 food sources during 60 h. An occupation ratio of the slime mold was computed per area as a quantification of the slime mold biomass distribution. We consider this biomass distribution as a weighted decision, inherently defined by a reinforcement process, even though its precise function is still to be formalised. For more information on the computation of the occupation ratio, refer to the Method section.
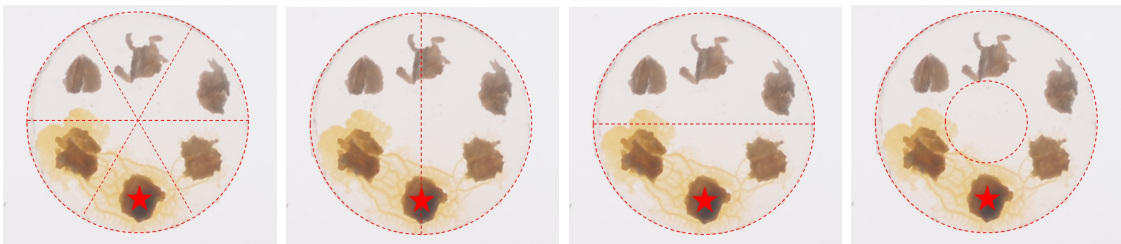
(a) Six food sources areas division   **(b)** Left and Right areas division   **(c)** Origin and Extremity areas division   **(d)** Inner and Outer areas division

Figure 4.1: Different areas layouts

Different groupings of areas in Fig 4.1 allow different analyses of this mass distribution. First, the dish was considered as 6 areas, one per food source. Each pixel belongs to the area of its closest food source, splitting the dish into 6 slices as in Fig 4.1a. Secondly, the timing of reinforcement will be analysed by comparing the origin and the exterior halves of the dishes; Thirdly, the symmetry will be examined from the left and right halves. Lastly, the food reinforcement will be studied by comparing the food-less inner circle with the rest of the dish.

4.1.1 Food sources areas

In this subsection are presented the results for the occupation ratio between the areas around the 6 food sources available to the slime mold as in Fig4.1a. Each area will be denoted according to its location :

- Origin : the inoculum noted with a star represents the original position of the slime mold before growth, also considered as the South pole.

- Extremity : area opposing the Origin, also considered as the North pole.
- Similarly to the two previous, all other areas are named after their cardinal location, South West, North West, South East and North East respectively.

4.1.1.1 Occupation Ratios

The occupation ratio of the 6 areas were computed by the estimated weight of physarum in each area divided by the area size. An even occupation ratio is thus 1/6, independently of small variations in experimental area size. In Fig 4.2, we note that each ratio rapidly converges to 1/6. From this quantification, no preference seems to emerge from the distribution. Independent of resource position in the dish, the occupation is evenly distributed over the areas of similar resource concentration.
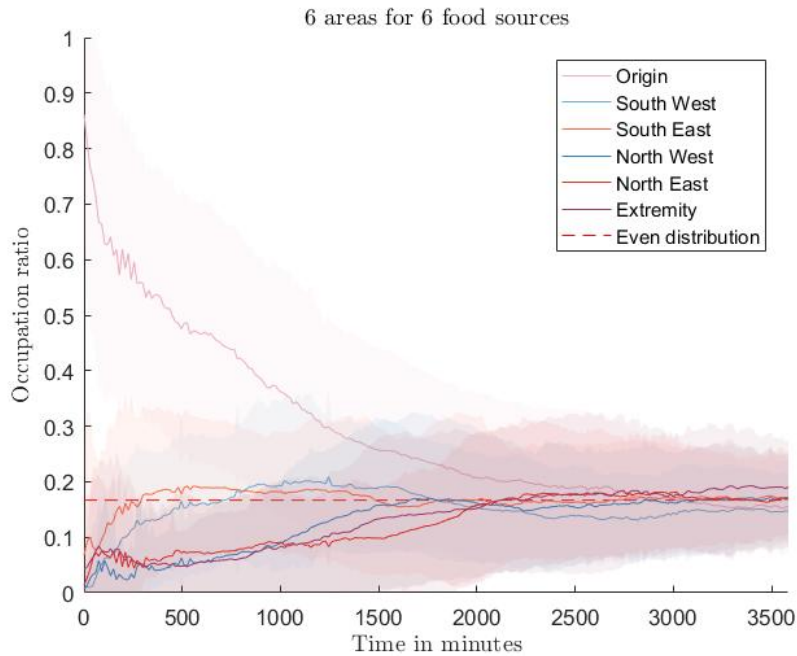
Figure 4.2: Occupation ratios of different areas

4.1.1.2 Dynamical convergence

To give an insight of the stability of such an even distribution state, the trajectory of the different averaged ratios was plotted in a phase plot in Fig 4.3. This kind of representation compares r, the ratio, with $\dot{r} = dr/dt$. A steady state is defined as $\dot{r} = 0$, points where the trajectories will eventually remain. The null hypothesis of an even distribution at steady state are plotted as a filled red dot in Fig 4.3 and the following graphs. Trajectories of r make loops around the steady state, suggesting that this equilibrium is stable. A stable steady state is defined as a steady state not affected by small perturbations. Indeed, small perturbations from the steady state would bring the trajectory back to the same point due to the converging loops around this point [30].
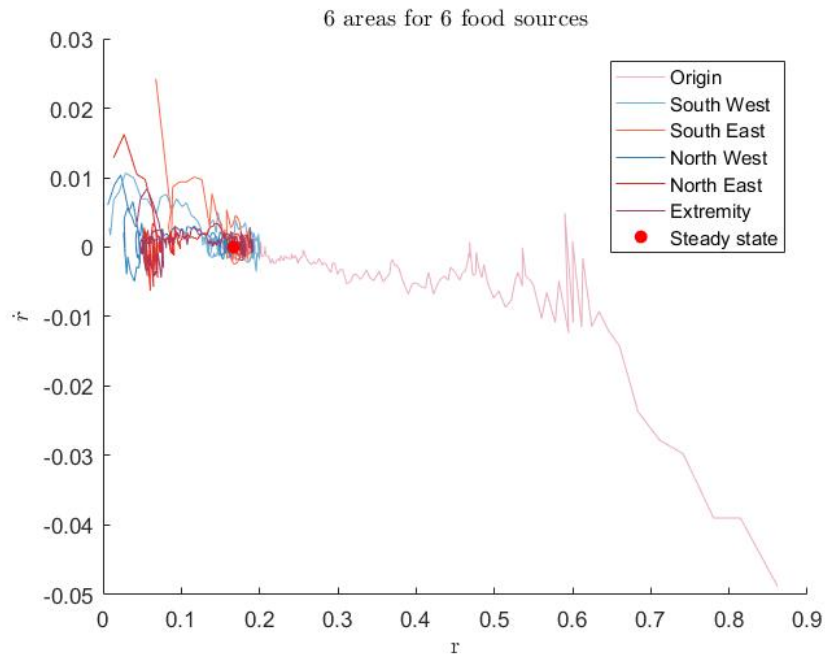
Figure 4.3: Ratios trajectory in the phase plane

4.1.2 Timing reinforcement

The experiments that follow explore the preference for food sources based on the timing of their encounter. We expect that while the Left vs Right ratios should be equal, the closer the food sources are from the original position, the more they are occupied. However, such observations were not made here, as the occupation ratio was not dependant of the distance from the inoculum. This could mean that there is no reinforcement due to timing, or that the measurements were not sensitive enough to quantify such difference.

4.1.2.1 Left vs Right asymmetry

In this section the results of the occupation ratio between the left and the right sides of the dish are examined for asymmetry as in Fig 4.1b. Each areas are denoted according to its location :

- Left : Corresponding to the West section in Fig4.1a. This area has been computed as all pixels closer to the left edge than the right edge.
- Right : Corresponding to the East section in Fig4.1a. This area has been defined as the opposite of the latter one.

The left and right sides possess even ratios (Fig4.4, however the steady state seems to be longer to reach. The oscillations around the even distribution seems to be less damped over time (Fig4.4 and 4.5). Nevertheless, as the area around the curve represents a single standard deviation, no firm difference can be drawn, as expected for this arrangement.
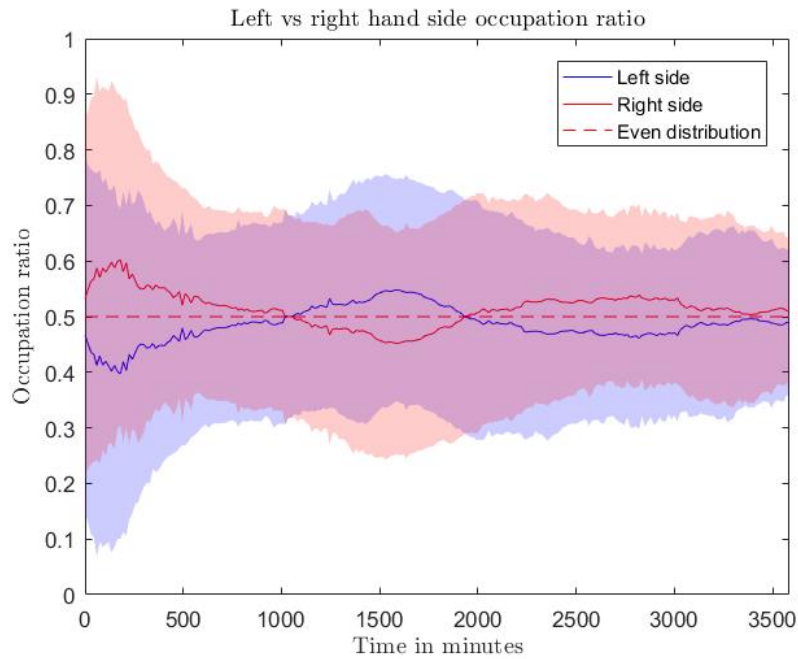
Figure 4.4: Occupation ratios of Left and Right areas
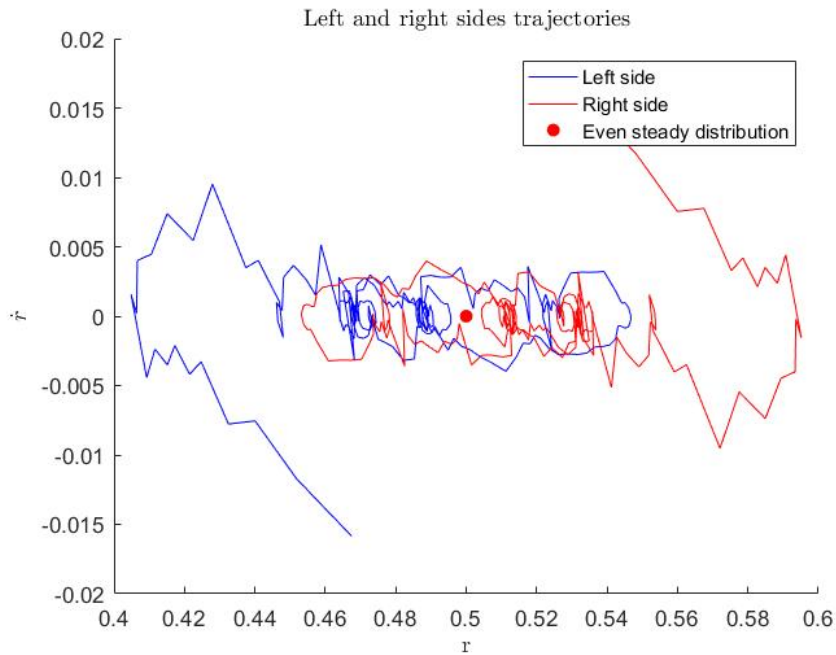
Figure 4.5: Left and Right ratios trajectory in the phase plane

4.1.2.2 Origin vs Extremity

In this subsection are exposed the results of the occupation ratio between the Origin and Extremity sides of the dish as in Fig4.1c. Each area was denoted according to its location :

- Origin : Corresponding to the South section in Fig4.1a. This area has been

computed as all pixels closer to the inoculum rather than the Northern edge.
- Extremity : Corresponding to the North section in Fig4.1a. This area has been defined as the opposite of the latter one.
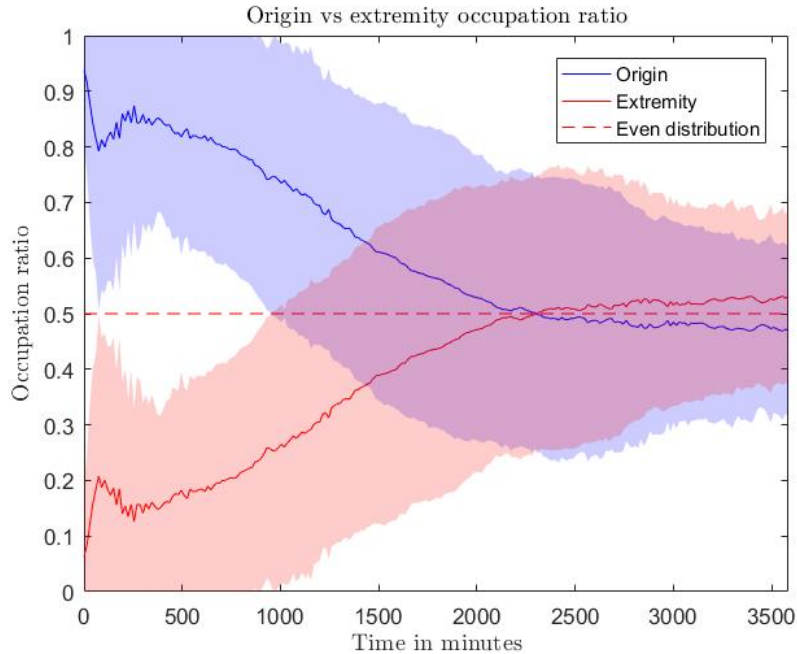
Figure 4.6: Occupation ratios of Origin and Extremity areas

The measurements here are critical for any hypothetical timing related reinforcement in the Physarum preferences. Nonetheless, as we can see in Fig 4.6 and 4.7, there was no clear difference between the area occupation ratios. This means that closer food sources are not preferred over more distant ones. More precisely if they are preferred, the occupation ratio is not sensitive enough to draw this conclusion.

4.1.3 Food reinforcement

In this subsection are shown the results of the occupation ratio between areas of different energetic values, respectively the internal and external disks shown as in Fig 4.1d. Each area will be denoted according to its location :
- Inner circle : This area has been defined as all the points closer to the centre of the dish than to another food sources. The centre of the dish is computed as the mean value of the six x and y food sources coordinates.
- Outer circle : This area has been defined as all the points closer to a food source than to the centre of the dish. one.

In this setup, the inner area is defined as an area without food sources. However, we can note that the ratio tends to equilibrium in fig4.8 and 4.9. The outer circle occupation seems to be slowly attracted by the steady state, yet it cannot be differentiated from the even distribution. This shows that the measurements used in this experimental protocol are not sensitive enough to draw any quantified and firm conclusion, as preference in resource-rich environments was expected to be observed.
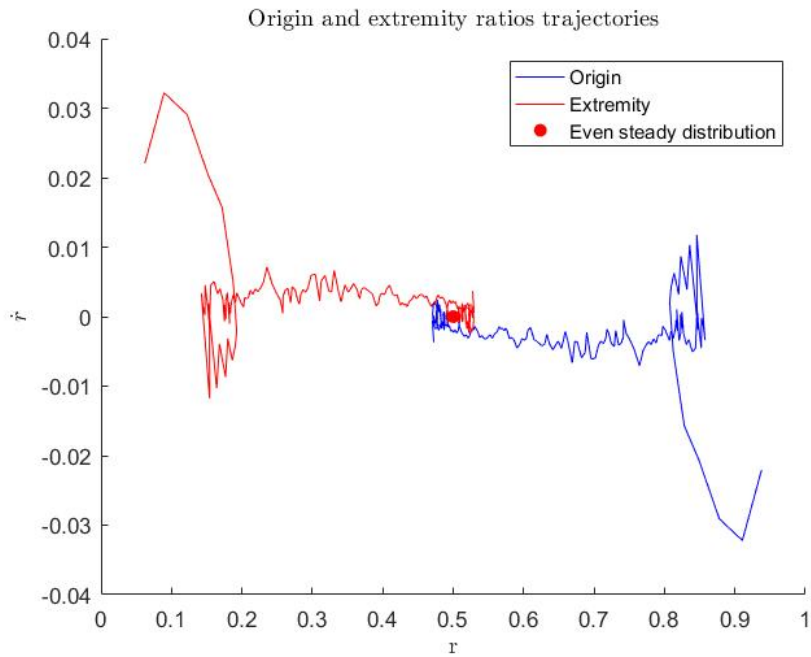
Figure 4.7: Origin and Extremity ratios trajectory in the phase plane
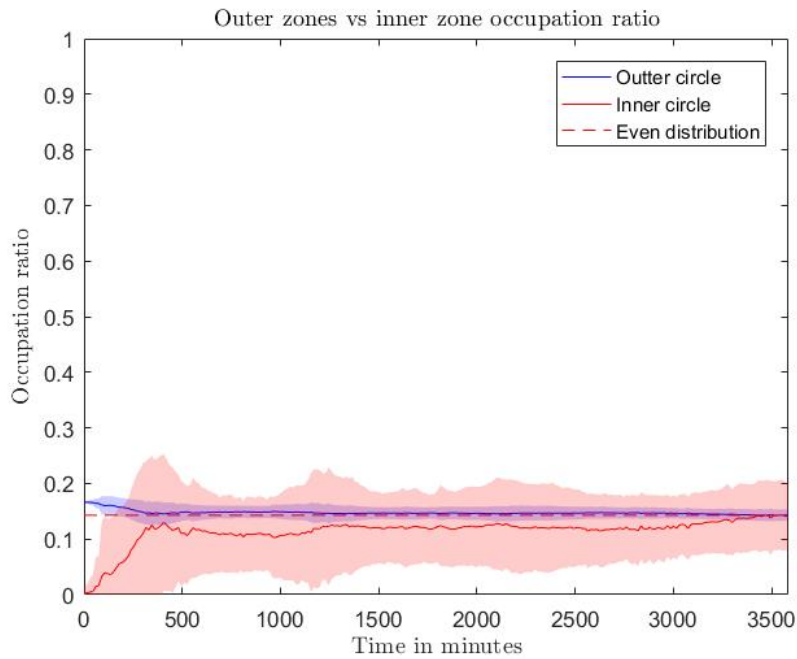
Figure 4.8: Occupation ratios of Inner and Outer areas

4.2 Importance of the cycle in the motion

No firm conclusions have drawn from the occupation ratios. The absence of significant difference between resource-rich areas and empty areas presented in Fig 4.8 suggests that this protocol is not sensitive enough. The rest of this thesis, and es-
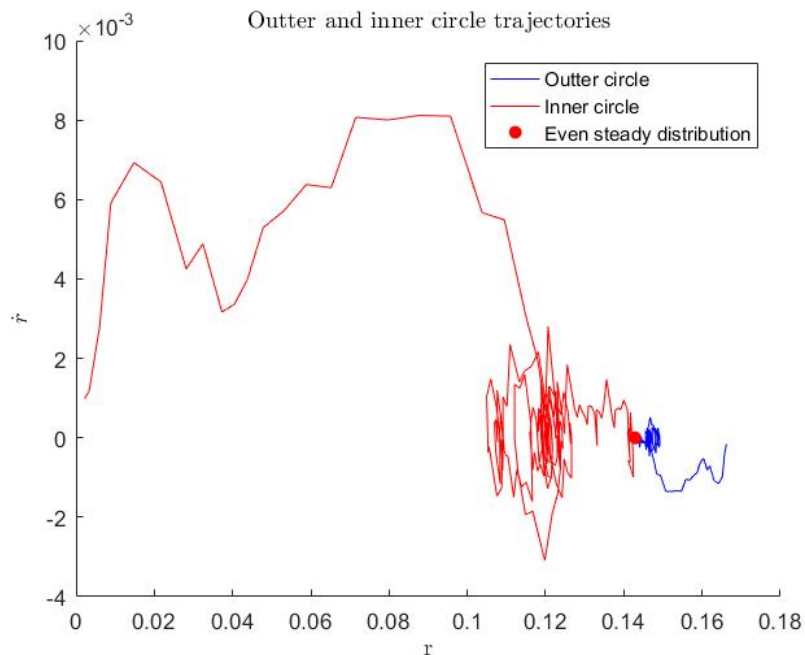
Figure 4.9: Outter and Inner ratios trajectory in the phase plane

pecially this section, will explore the quantification of flow within the veins using microscopy and fluorescent beads. The first section will focus on the contractile motions of the veins, and their role in the flow analysis. The second section will focus on the comparison of the theoretical and experimental data.

4.2.1 Contractile motion

The contractile motions of Physarum are well documented [21, 31, 26]. A contractile cycle of 120 s is known to drive peristaltic flow within the veins, alternating its orientation via *shuttle streaming* [32, 14].

This contractile pattern may coexist with other rhythmic patterns of lower frequencies. As these contractile motions directly impact the radius, and more importantly the derivative of the conductivity dD_{ij}/dt, it is important to study their roles. The contractile motions are not modelled by the Flow Conductivity Model [5], even if this model heavily depends on the resulting conductivity changes. The biological role of those cycles is fundamental to the organism, but putting them aside from a model could may be a reasonable choice for computational costs issues. To assess the importance of such cycles, we need to further investigate these contractions, which is the aim of this section.

4.2.2 Decomposition of the signal

4.2.2.1 Obtaining a signal from a radius

The radius of each veins showed both complex oscillations and global trends. For each radius, we extracted its trend using a moving mean from the time series and

then subtracting it from the original curve to give it more stationnary oscillations as in Fig 4.10. We then obtained a de-trended signal R_{ij}' suitable for analysed using a Fourier transform.
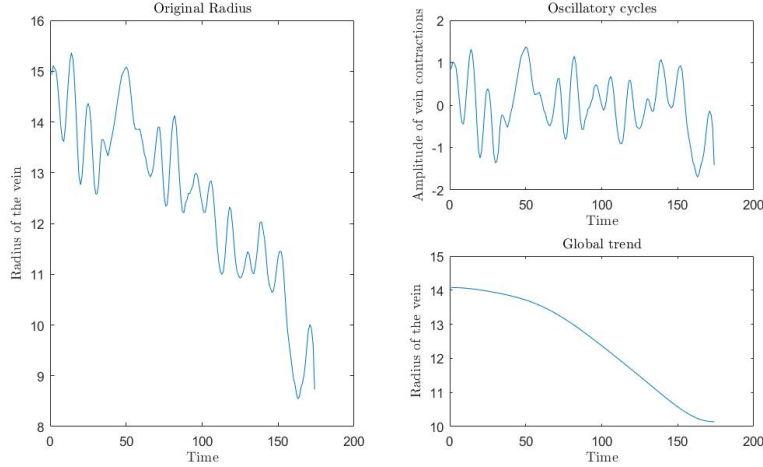
Figure 4.10: Decomposition of the radius into a signal and trend

To study the rhythmic variations of the vein size, we decomposed the radius into several Fourier components. Using a Fourier transform allowed us to extract μ cycles having the highest amplitude. The relevant number of frequencies to extract depends on the nature of the data. Once the μ more important cycles have been extracted, we can use an inverse Fourier transform to express R_{ij}' as :

$$R_{ij}'(t) = \sum_{\nu=1}^{\mu} m_{ij}^{\nu} \cos\left(2\pi \cdot f_{ij}^{\nu} \cdot t + \phi_{ij}^{\nu}\right) \tag{4.1}$$

With $R_{ij}(t) = R_{ij}'(t) + R_{ij}^{MM}(t)$, where $R_{ij}^{MM}(t)$ is the moving mean trend

In equation 4.1 $R_{ij}'(t)$ is the radius of the vein ij at time t, and where ν is the index of the Fourier components used to simplify the signal (here up to μ components). While f, m and ϕ refer to the frequency, magnitude, and phase of each Fourier component respectively.

4.2.2.2 Choosing the number μ of components to extract

The choice of μ in equation 4.1 depends not only on the signal, but also on the coherence between the different veins. Indeed, as the same process is repeated independently for each vein ij, coherence in the frequencies selected is of interest. However, a high number of components μ will increase the model accuracy, as more subtle changes would be taken into account. This trade-off has been addressed by observing the overlaps in the different frequencies, and the concordance of the modelled radius with the actual radius. The concordance has been computed by the probability of the two derivatives of being of the same sign and is showed in Fig 4.11.
We decided to extract 2 components, $\mu = 2$ in equation 4.1. NOte that decreasing μ would lead to a very low concordance (from 68% to 50%), whilst increasing μ did

not significantly improve it (from 68% to 69%). As we can see in Fig 4.11, a cyclic pattern appears in the concordance over time, meaning that some cycles were badly scaled or excluded. However, we will consider this noise as irrelevant because of the quality of the non-overlapping frequencies found in Fig4.12.
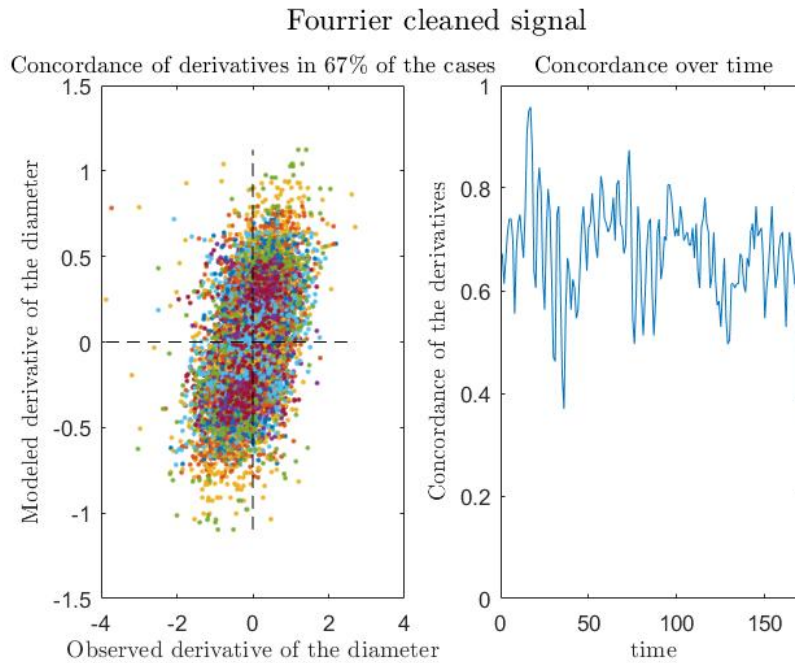
Figure 4.11: Concordance of a signal with $\mu = 2$ components

The frequencies of oscillations are remarkably coherent from one vein to another when the signal is decomposed in two components (Fig 4.12). Their magnitudes are similar, which suggests that the contribution of each cycle is similar on the final radius. The fast cycle is composed of an average of 15 oscillations in 1886 s (31 min). This fast cycle corresponds to the flow oscillation cycle of period about 125 s referred in the literature [21, 31, 26, 14, 32]. The slower cycle, having a period of about 8 to 10 min, is less well documented, though it has a similar amplitude as the fast one (Fig 4.12).

4.2.3   Phase and timing

4.2.3.1   Visualisation of the flow

We know that the fast cycle has an important role in driving the flow, but the physics of its actual behaviour is still unclear [14]. In Fig4.13, the flow speed is plotted against variations in the radius. The size of the circles is related to the speed of the flow (independently of its orientation). We can visually tell that the flow often occurred at extreme radii, and especially when the radius was sharply increasing. Those sharp increases corresponded to the fast cycle of period 120 s. The verification of this observation was made using the Fourier's component phases we obtained in Fig4.12.
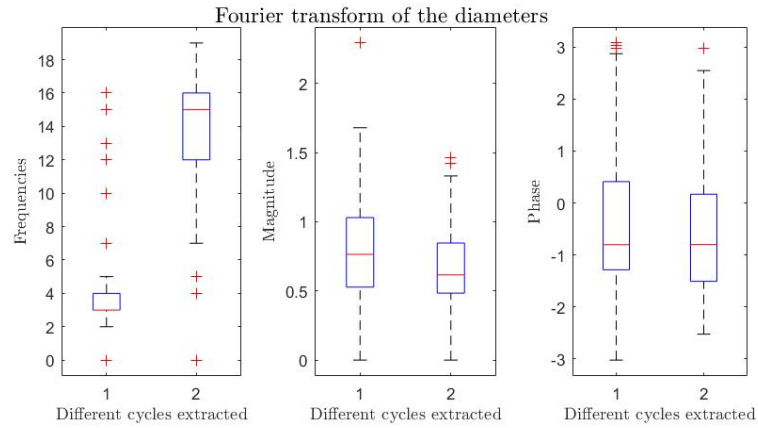
Figure 4.12: Parameters of the two Fourier components
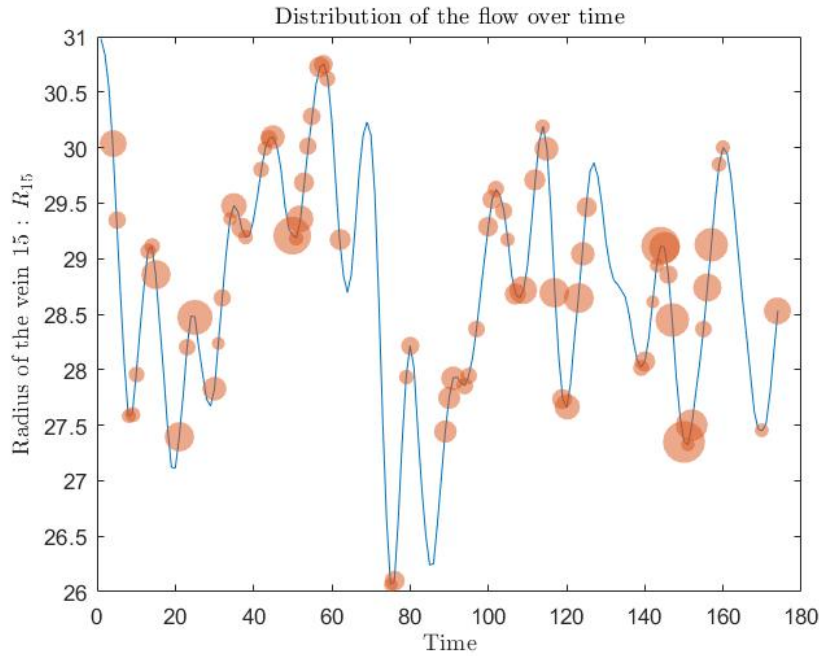
Figure 4.13: Speed of the flow and radius of vein 15

4.2.3.2 Phase distribution

In this section, we quantify the distribution of the flow within the different phases of the Fourier's components. The intuition is that the flow is driven when the fast cycle is in an opening phase. To do so, the phases of the two components were extracted as follow :

$$\theta_{ij}^{\nu}(t) = 2\pi \cdot f_{ij}^{\nu} \cdot t + \phi_{ij}^{\nu}$$

Where $\theta_{ij}^{\nu}(t)$ is the phase of each component ν in vein ij at the moment t when a bead is passing faster than a nominal threshold of $23\,\mu\text{m/s}$, to reduce the noise of the data. The distribution of θ^{ν} is made in Fig4.14.

To interpret the results in Fig 4.14, one must recall that the terms summed in eq

Phase distribution when fast beads are passing through the vein (With Omnibus test)
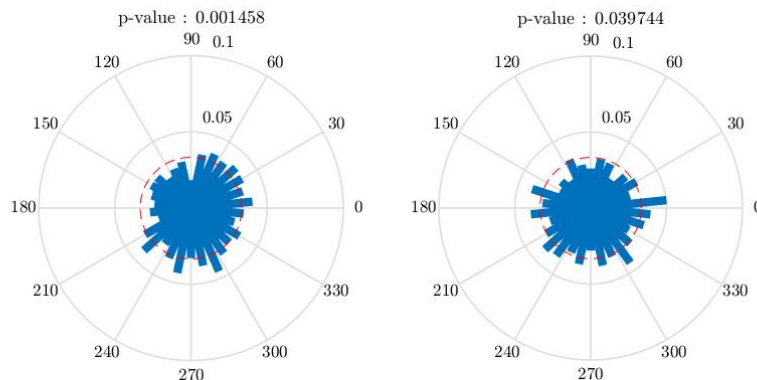
Figure 4.14: Distribution of phases during fast passing beads events

4.1 are cosines. Meaning that each cycle ranges from m^ν (its amplitude) at phase $\theta^\nu = 0$ to $-m^\nu$ at $\theta^\nu = \pi$. Thus in Fig 4.14, the angles from 0 to π (upper part of the graph), represent the closing phase of the cycle that reaches its lowest value $-m^\nu$ at $\theta^\nu = \pi$. And similarly, veins are opening when θ^ν is between $-\pi$ and 0 (lower part of the graph), reaching their highest values m^ν at $\theta^\nu = 0$.

The even distribution is plotted in Fig4.14 as red dashed lines. Omnibus tests for uniform angle distributions were carried out, and the results are significantly rejecting an uniform distribution ($p^1 = 0.001458$ and $p^2 = 0.039744$). Fast flow events are more likely when the slow cycle on the left is wide open. On the other hand, fast flow events are more likely when the fast cycle on the right is dilating.

These results could be interpreted as a slow rhythm giving a minimum size for the beads to flow within the veins. Whilst the opening motion of the fast cycle are used as a driving force for the beads. This driving force seems based on local opening rather than the contraction of the veins, which is biologically surprising. However, the relaxation observed during opening is most likely driven by contraction elsewhere in the system.

4.2.4   Phase shift and reinforcement

Knowing that the physics of the fast contractions are leading the flow, the role of the slow cycle still needs to be defined. We proposed in Fig 4.15 a visualisation that could underline its importance.

In Fig4.15 the average variation of radius $< dR_{ij}/dt >$ was compared to the initial phase distribution ϕ_{ij}^ν in the eq 4.1. The average radius variation shows whether a vein is decaying in average (blue) or growing (and being selected) (yellow), using the sign of $< dR_{ij}/dt >$. We can note that the growing veins are not synchronised with the rest of the veins on the slow cycle, while still being synchronised on the
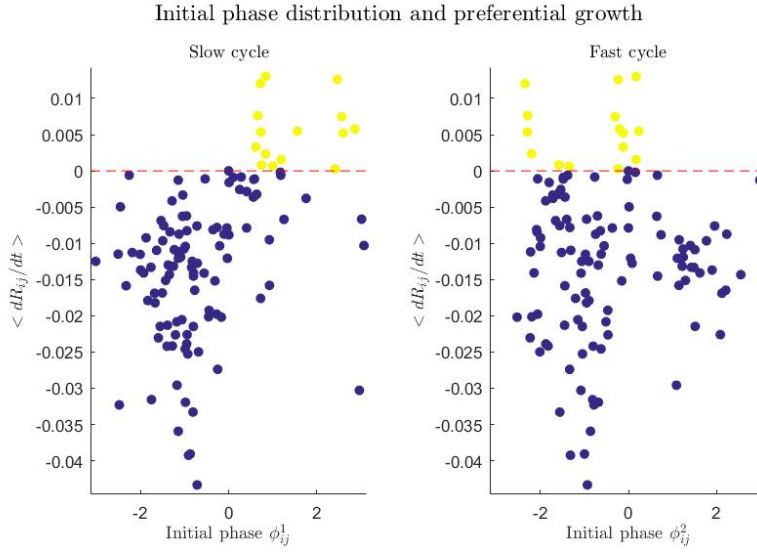
Figure 4.15: Long term growth preferences based on initial phase ϕ_{ij}^{ν}

fast cycle. Not only are they synchronised, they seem to be off-beat. Which would mean that the slow cycle allows to differentiate the veins to select from the ones to let decay over time; while the fast cycle (creating the flow) could be used to transfer the body mass from decaying veins to the growing ones.

4.3 Flow Conductivity Model parameterisation

4.3.1 Re-scaling

The conductivity variations caused by the contractile cycles are too wide to be considered in the new Flow Conductivity Model. As the Flow Conductivity Model consists of explaining conductivity variation by flow reinforcement over a longer time period, wide and short term oscillations may just bring noise to the system. Besides, those oscillations are often wider than the overall vein radius change over the 30 minutes span of the experiment. The measurement of the conductivity D_{ij} of an edge (of a vein) between two nodes i and j has been carried as follow :

$$D_{ij}\left(t\right) = \frac{\pi R_{ij}^4\left(t\right)}{8\xi} \tag{4.2}$$

For the sake of the computation, we estimated a viscosity $\xi = 1$, assuming it is of the same order as water.
The absolute flow in the vein ij was determined by measurement of the speed of beads $v_{ij}^{max}(t)$ multiplied by the cross section area of the vein (assumed to be circular and ocntinous along the vein). The term $v_{ij}^{max}(t)$ refers to the highest speed of bead observed in vein ij in timestep t. As we are assuming a Poisseuille flow, the distance between the bead and the centre of the vein affects the speed of the bead. So for better measurements of the flow we only included the fastest bead of each time steps

as follows :

$$|Q_{ij}(t)| = v_{ij}^{max}(t) \cdot \pi R_{ij}(t)^2 \tag{4.3}$$

4.3.2 Research of parameters

The effect of varying parameters μ and α of the Flow Conductivity Model have been carried out exhaustively between certain intervals (0 to 5). The simulation results do not fit the data, irrespectively of the different $f(|Q_{ij}|)$ cases proposed in the literature :

$$f(|Q_{ij}|) = \begin{cases} |Q_{ij}|, \text{ case (1)} \\ |Q_{ij}|^{\mu}, \text{ case (2)} \\ \frac{Q_{ij}^{\mu}}{1+Q_{ij}^{\mu}}, \text{ case (3)} \end{cases}$$

Indeed, in Fig 4.16 (with $\mu = 1.425$ and $\alpha = 0.05$) the trend of dD_{ij}/dt exponentially diverges from the real data curve, even if the overall trend seems to be matching the growth. The matching trend could explain why this formula still exhibit interesting features in the modelling done in the literature.
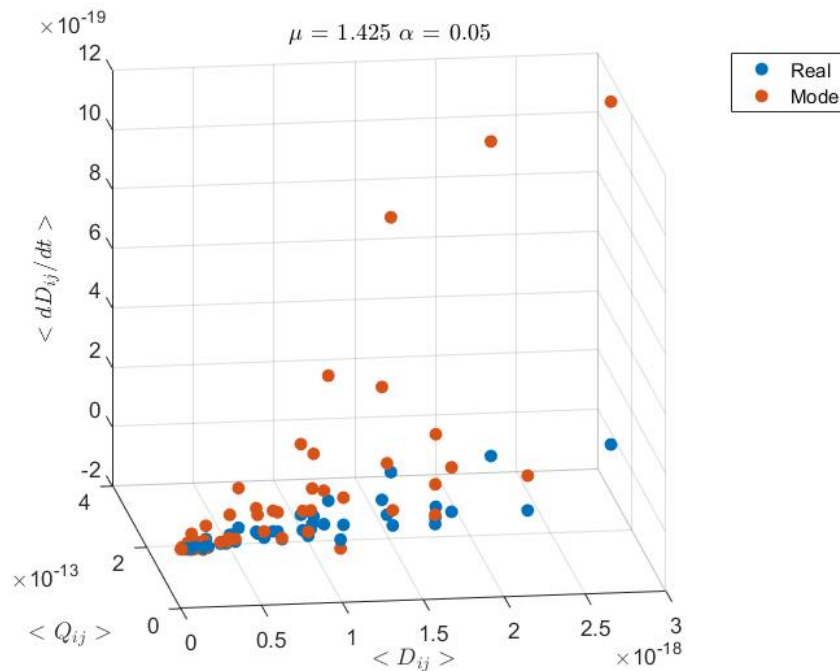
Figure 4.16: Flow Conductivity Model's optimal parameters

Estimation of these parameters have also been carried using the `cftool` toolbox in Matlab. This toolbox did not give better results that the one we already shown in fig4.16.

4.3.3 Proposal

The Flow Conductivity Model did not match the experimental data, but the set of points we obtained experimentally was fitted according to a new formula. A good prediction model of dD_{ij}/dt was found empirically using the curve fitting toolbox `cftool` in Matlab. The fit is displayed on Fig4.17 and expressed as :

$$dD_{ij}/dt = \alpha + \beta D_{ij} + \gamma|Q_{ij}| + \zeta\left(|Q_{ij}| \cdot D_{ij}\right) + \eta|Q_{ij}|^2 \tag{4.4}$$

With,
$$\begin{cases} \alpha = -1.196e^{-22}, & IC_{95\%} = (-1.624e^{-22}, -7.681e^{-23}) \\ \beta = -0.002332, & IC_{95\%} = (-0.002597, -0.002066) \\ \gamma = 1.72e^{-8}, & IC_{95\%} = (1.33e^{-8}, 2.11e^{-8}) \\ \zeta = 3.282e^{10}, & IC_{95\%} = (3.012e^{10}, 2.553e^{10}) \\ \eta = -2.338e^{5}, & IC_{95\%} = (-2.619e^{5}, -2.057e^{5}) \end{cases}$$
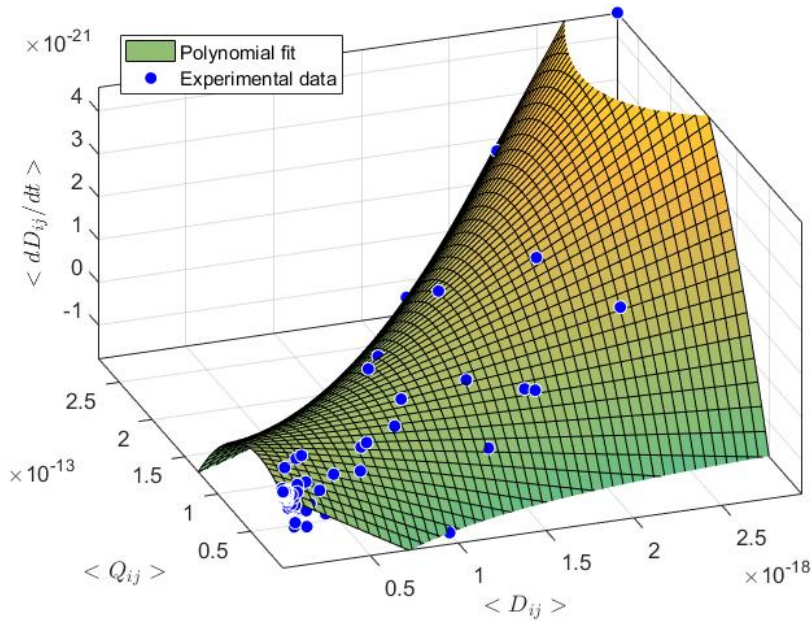
Figure 4.17: Polynomial fit proposed

The parameters of the equation 4.4 were fitted to the experimental data. However, the function itself is not biologically inspired, and parameters do not correspond to intuitive functions like in the Flow Conductivity Model. One can note that β had a similar negative decay role based on the conductivity, similarly to α in the Flow Conductivity Model. However, the more significant parameters here, η and ζ, do have an obvious biological correlate, or more precisely do not bring more knowledge about the system biologically than the previous models did.

5

Discussion

Working question : What is the reinforcement process in Physarum's decision making?

5.1 Initial condition and timing

Sub Question 1 : Is the reinforcement sensitive to initial conditions or timing of resource encounter?

The expansion of the slime mold, and the order in which it meets food sources had no influence on its decision process. Nonetheless, the analysis metric or the experimental scale used are probably not sensitive enough to determine such bias. The occupation ratio computed at this scale was not different from the spread of a viscous liquid reaching an even distribution after some time. The occupation ratio may be more critical when measuring the food source occupation rather than the space occupation [9]. However, in our case, as the food sources are opaque, we could not compute a reliable occupation of these specific points. This problem could be tackled by using different translucent food sources or by improving the segmentation. Notably, the visualisation could have been improved by using food colouring [26]. However, its impact on the Physarum's behaviour is unknown.

5.2 Modelling experimental data

Sub Question 2 : Is the current reinforcement model consistent with the experimental data? if so, what are the parameters providing the best fit?

5.2.1 Absence of oscillation

The absence of oscillation in the Flow Conductivity Model is perhaps surprising, as it is one of the key physiological elements of Physarum [32]. The study of these oscillations in this thesis has however shown, that their role is likely to be important in vein selection. Indeed, using an approximation of the radius variation by two Fourier components, we show that the phase of slow oscillations may discriminate growing veins from decaying ones, whilst fast oscillations physically drive the flow. If the implications of the oscillations in the vein selection process are as important as quantified in this thesis, a Physarum model implementing a shuttle streaming might be an improvement. The Flow Conductivity Model currently lacks a key element in

its simulation, not only to be biologically coherent, but probably also to be efficient in its vein selection.

Nonetheless, in the scope of biological relevance, our results might be nuanced in many ways, as a high flow associated with widening veins instead of contracting them is highly counter-intuitive, and implies contractions elsewhere in the system that were not recorded.

It is important to note also that the slime mold may try to escape the bright area of the microscope, which could influence the vein selection. A better quantification of the quality of the Fourier transform is also essential, as our *concordance*(Fig4.11 page 23) was made to give fast, but approximate results. The correlation of the residuals is clearly a sign of possible improvement to the overall reliability of our model.

5.2.2   Convenient fitting

The model does not fit the data in any of the current forms of $f\left(|Q_{ij}|\right)$ used, whilst a newly proposed model can fit the data (eq 4.4, Fig4.17, pages 28 and 28). The new model does not have any biological significance per se and could thus be the result of data over-fitting. More importantly it is usefel to discuss the role and the parameters present in a model in general to give us more knowledge about the system.

On another hand, the new model proposed in 4.4 needs 5 parameters from completely different scales; where the Flow Conductivity Model only possess two parameters of the same scale. Thus, even if the Flow Conductivity Model is not strictly accurate biologically, we can still say that it is more convenient, and gives a better pedagogical insight into the slime mold's capacities and behaviour. In the scope of applied optimisation problems, the Flow Conductivity Model will probably be a better candidate than our new model. Although, applying the experimentally found parameters to the model is a natural continuation of this thesis that would need further investigation.

6

Conclusion

The Flow Conductivity Model is not an accurate description of the biological reality
- it is missing plasmodium extension and food foraging behaviours
- there has been no experimental calibration of the parameters
- the contractile cyclic motions are not included

However, the experiments carried in this thesis show that the expansion of the plasmodium does not play an important role in the food source selection at the macroscale. Indeed, the order in which the food sources are met does not affect the final output, making inclusion of the expansion an expensive process to simulate without any clear benefit. It is thus not necessary to implement it in the model.

Secondly, the parameter calibration does not match the experimental data, and the flow does not seem to reinforce the veins in the way previously proposed, even if the trend is similar. Further experimentation and modelling show that other models could fit the data better. However, the reviewed model does not bring additional semantic value, as it does not summarise the actual behaviour of the slime mold in a comprehensive way. In other words, this new model did not teach us anything more about the slime mold, and does not have the benefice of being simpler either.

Finally, this thesis exposed interesting properties about the contractile motion. Mainly, two rhythmic contractile motions have been noted coherently between all the veins, each of them having their role in the flow and the vein selection. Our experiments would suggest that the flow is carried by fast and cyclic vein widening; while slow oscillations would act as a gate, allowing flow only when wide open. The slowest rhythmic cycle seems to play a role in the selection of veins, as preferred growing veins are off-rhythm with the others, while still being synchronised on the fast cycle.

The contractile motion behaviour observed experimentally would be of interest in a model. Nonetheless, the random sink and source alternation in the Flow Conductivity Model arises random alternating flows that still allow correct edges to be selected over others. In this sense, oriented randomness besides being simpler to implement than non linear pulsing dynamics, still exhibits desired behaviour, namely edge selection.

If the Flow Conductivity Model lacks experimental support, it still satisfies both optimisation objectives and pedagogical purposes. The experimental protocols we developed during this thesis using fluorescence and Fourier Transforms would need further exploration, and may be promising for other network systems (for instance fungi networks). Indeed, it gives interesting insight of the biology and bio-mechanic of such local behaviour, providing a full set of metrics for subsequent modelling.

In conclusion, the experiments in this thesis could not formalise an overall reinforce-

ment process in Physarum's vein selection. Nevertheless, evidence concerning the roles of the oscillatory cycles in vein's selection has been emphasised. These cycles are good candidates to explain Physarum's decision making process, despite the fact that they are not included in the state-of-the-art Flow Conductivity Model. The importance of those cycles may be subject to further studies.

Bibliography

[1] David Frisk. A Chalmers University of Technology Master's thesis template for LATEX. page 3.

[2] A. Perna and T. Latty. Animal transportation networks. *Journal of The Royal Society Interface*, 11(100):20140334–20140334, August 2014.

[3] Eleni Katifori, Gergely J. Szöllősi, and Marcelo O. Magnasco. Damage and Fluctuations Induce Loops in Optimal Transport Networks. *Physical Review Letters*, 104(4), January 2010.

[4] Guénaël Cabanes, Ellen van Wilgenburg, Madeleine Beekman, and Tanya Latty. Ants build transportation networks that optimize cost and efficiency at the expense of robustness. *Behavioral Ecology*, 26(1):223–231, 2015.

[5] A. Tero, S. Takagi, T. Saigusa, K. Ito, D. P. Bebber, M. D. Fricker, K. Yumiki, R. Kobayashi, and T. Nakagaki. Rules for Biologically Inspired Adaptive Network Design. *Science*, 327(5964):439–442, January 2010.

[6] JesúS GóMez-GardeñEs and Yamir Moreno. SYNCHRONIZATION OF NETWORKS WITH VARIABLE LOCAL PROPERTIES. *International Journal of Bifurcation and Chaos*, 17(07):2501–2507, July 2007.

[7] Marco Dorigo, Vittorio Maniezzo, and Alberto Colorni. The Ant System: Optimization by a colony of cooperating agents. page 26, 1996.

[8] Liping Zhu, Song-Ju Kim, Masahiko Hara, and Masashi Aono. Remarkable problem-solving ability of unicellular amoeboid organism and its mechanism. *Royal Society Open Science*, 5(12):180396, December 2018.

[9] A. Dussutour, T. Latty, M. Beekman, and S. J. Simpson. Amoeboid organism solves complex nutritional challenges. *Proceedings of the National Academy of Sciences*, 107(10):4607–4611, March 2010.

[10] Toshiyuki Nakagaki, Atsushi Tero, Ryo Kobayashi, Isamu Onishi, and Tomoyuki Miyaji. Computational Ability of Cells based on Cell Dynamics and Adaptability. *New Generation Computing*, 27(1):57–81, November 2008.

[11] Atsushi Tero, Ryo Kobayashi, and Toshiyuki Nakagaki. Physarum solver: A biologically inspired method of road-network navigation. *Physica A: Statistical Mechanics and its Applications*, 363(1):115–119, April 2006.

[12] Atsushi Tero, Toshiyuki Nakagaki, Kazutaka Toyabe, Kenji Yumiki, and Ryo Kobayashi. A method inspired by Physarum for solving the Steiner problem. *International Journal of Unconventional Computing*, 6(2):109–123, 2010.

[13] Atsushi Tero, Ryo Kobayashi, and Toshiyuki Nakagaki. A mathematical model for adaptive transport network in path finding by true slime mold. *Journal of Theoretical Biology*, 244(4):553–564, February 2007.

[14] K. Alim, G. Amselem, F. Peaudecerf, M. P. Brenner, and A. Pringle. Random network peristalsis in Physarum polycephalum organizes fluid flows across an individual. *Proceedings of the National Academy of Sciences*, 110(33):13306–13311, August 2013.

[15] Soichiro Tsuda and Jeff Jones. The emergence of synchronization behavior in Physarum polycephalum and its particle approximation. *Biosystems*, 103(3):331–341, March 2011.

[16] Thilo Gross and Hiroki Sayama, editors. *Adaptive networks: theory, models and applications*. Understanding complex systems. Springer, Dordrecht ; New York, 2009. OCLC: ocn401151178.

[17] Tomoyuki Miyaji and Isamu Ohnishi. PHYSARUM CAN SOLVE THE SHORTEST PATH PROBLEM ON RIEMANNIAN SURFACE MATHEMATICALLY RIGOROUSLY. page 18.

[18] T. Ohta, S. Kawano, and T. Kuroiwa. Fine Structure of Centrosome Complex and its Connection with Cell Nucleus in the Slime Mould, Physarum polycephalum. *CYTOLOGIA*, 57(4):515–523, 1992.

[19] E. Meijering, M. Jacob, J.-C.F. Sarria, P. Steiner, H. Hirling, and M. Unser. Design and validation of a tool for neurite tracing and analysis in fluorescence microscopy images. *Cytometry*, 58A(2):167–176, April 2004.

[20] Brian J Harrington and Kenneth B Raper. Use of a Fluorescent Brightener to Demonstrate Cellulose in the Cellular Slime Molds. *APPL. MICROBIOL.*, 16:8, 1968.

[21] Shun Zhang, Robert D Guy, Juan C Lasheras, and Juan C del Álamo. Self-organized mechano-chemical dynamics in amoeboid locomotion of *Physarum* fragments. *Journal of Physics D: Applied Physics*, 50(20):204004, May 2017.

[22] Dirk Dormann and Cornelis J Weijer. Propagating chemoattractant waves coordinate periodic cell movement in Dictyostelium slugs. page 9.

[23] Jens Rietdorf, Florian Siegert, and Cornelis J. Weijer. Analysis of Optical Density Wave Propagation and Cell Movement during Mound Formation in Dictyostelium discoideum. *Developmental Biology*, 177(2):427–438, August 1996.

[24] J. Saragosti, V. Calvez, N. Bournaveas, B. Perthame, A. Buguin, and P. Silberzan. Directional persistence of chemotactic bacteria in a traveling concentration wave. *Proceedings of the National Academy of Sciences*, 108(39):16235–16240, September 2011.

[25] N. Otsu. A Threshold Selection Method from Gray-Level Histograms. *IEEE Transactions on Systems, Man, and Cybernetics*, 9(1):62–66, January 1979.

[26] Toshiyuki Nakagaki, Hiroyasu Yamada, and Tetsuo Ueda. Interaction between cell shape and contraction pattern in the Physarum plasmodium. *Biophysical Chemistry*, 84(3):195–204, May 2000.

[27] Alejandro F. Frangi, Wiro J. Niessen, Koen L. Vincken, and Max A. Viergever. Multiscale vessel enhancement filtering. In William M. Wells, Alan Colchester, and Scott Delp, editors, *Medical Image Computing and Computer-Assisted Intervention — MICCAI'98*, Lecture Notes in Computer Science, pages 130–137. Springer Berlin Heidelberg, 1998.

[28] Norbert Wiener and Mass) Massachusetts Institute of Technology (Cambridge. *Extrapolation, interpolation, and smoothing of stationary time series: with engineering applications.* Technology Press, 1950.

[29] Irwin Sobel and Gary Feldman. A 3x3 isotropic gradient operator for image processing. *a talk at the Stanford Artificial Project in*, pages 271–272, 1968.

[30] Steven H. Strogatz. *Nonlinear dynamics and Chaos: with applications to physics, biology, chemistry, and engineering.* Studies in nonlinearity. Addison-Wesley Pub, Reading, Mass, 1994.

[31] M. Radszuweit, H. Engel, and M. Bär. A model for oscillations and pattern formation in protoplasmic droplets of Physarum polycephalum. *The European Physical Journal Special Topics*, 191(1):159–172, December 2010.

[32] Toshiyuki Nakagaki, Hiroyasu Yamada, and Masami Ito. Reaction–Diffusion–Advection Model for Pattern Formation of Rhythmic Contraction in a Giant Amoeboid Cell of thePhysarumPlasmodium. *Journal of Theoretical Biology*, 197(4):497–506, April 1999.